Journal of Magnetic Resonance 302 (2019) 64–71

Contents lists available at ScienceDirect

Journal of Magnetic Resonance

journal homepage: www.elsevier.com/locate/jmr

Real-time pure shift measurements for uniformly isotope-labeled molecules using X-selective BIRD homonuclear decoupling

Jens D. Haller [a], Andrea Bodor [b], Burkhard Luy [a,*]

[a] Institut für Organische Chemie and Institut für Biologische Grenzflächen 4 – Magnetische Resonanz, Karlsruher Institut für Technologie (KIT), Fritz-Haber-Weg 6, 76133 Karlsruhe, Germany

[b] Eötvös Loránd University, Institute of Chemistry, Laboratory of Structural Chemistry and Biology, Pázmány Péter sétány 1/a, Budapest 1117, Hungary

ARTICLE INFO

Article history:
Received 27 February 2019
Revised 28 March 2019
Accepted 29 March 2019
Available online 30 March 2019

Keywords:
Inversion element
Band selective
Homonuclear decoupling
BIRD
Real-time
Pure shift
Isotope-labeling
BASEREX

ABSTRACT

We introduce a novel selective inversion element for chunked homonuclear decoupling that combines isotope selection via BIRD-filtering with band-selective inversion on the X-heteronucleus and allows efficient real-time decoupling of homonuclear and heteronuclear couplings. It is especially suitable for uniformly isotope-labeled compounds. We discuss in detail the inversion element based on band-selective refocusing on the X-nuclei (BASEREX), highlighting in particular the role of appropriate band-selective shaped refocusing pulses and the application of broadband X-pulses for an effective BIRD^{d} element during homodecoupling. The approach is experimentally verified and studied in detail using uniformly ^{13}C-labeled glucose and a uniformly ^{15}N,^{13}C-labeled amino acid mixture.

1. Introduction

The simplification of spectra is a long-standing goal in NMR spectroscopy. In particular, the removal of splittings due to scalar couplings has found widespread applications and the development of corresponding decoupling methods is still in full swing. While heteronuclear decoupling can be accomplished in real-time by the irradiation of composite pulse decoupling sequences during acquisition [1–5], homonuclear decoupling requires more elaborate approaches. Reconstruction of decoupled spectra from an additional pseudo-dimension has been initially introduced in J-spectroscopy [6,7] and later combined with more elaborate techniques [8–14], while first real-time approaches involved stroboscopic irradiation of a band-selective decoupling sequence during acquisition [1,15–21]. Following the seminal paper of Zangger and Sterk [22], however, a multitude of chunking-based interferogram [13,23–32] and real-time approaches [33–37] have been developed during the last decade that have revolutionized the field.

As has been nicely summarized in Refs. [35,38,39], the different homodecoupling methods based on appropriate chunking can be classified according to their elements used for selective inversion, which can either result in broadband or band-selective decoupling. While broadband decoupling schemes like the original Zangger-Sterk [22] or the PSYCHE-based approaches [40,41], will result in significantly reduced sensitivity, corresponding band-selective approaches like the HOBS [42] or BASHD [43] experiments do not come with this inherent penalty and might even increase the overall signal-to-noise-ratio. Homonuclear decoupling based on isotope-selective, broadband BIRD [8,24,26–28,44,45] inversion, as a third kind of selective inversion element, depends on the presence of a low-abundance isotope and leads to a reduction of sensitivity according to the concentration of the filtered X-nucleus. The technique will fail, however, in the case of uniformly isotope-labeled compounds, if coupled spins are inverted simultaneously.

Here, we present a different approach that is based on the combination of isotope- and band-selective inversion that allows real-time homonuclear decoupling also in the case of uniformly isotope-labeled molecules. The BIRD-homodecoupling based on band-selective refocusing on the X-nuclei, termed BASEREX, is introduced and compared to other BIRD-homodecoupling methods. In addition, the effect of heteronuclear coupling evolution on the right choice of band-selective pulses is studied using average

* Corresponding author at: Institut für Organische Chemie and Institut für Biologische Grenzflächen 4 – Magnetische Resonanz, Karlsruher Institut für Technologie (KIT), Fritz-Haber-Weg 6, 76131 Karlsruhe, Germany.
E-mail address: burkhard.luy@kit.edu (B. Luy).

https://doi.org/10.1016/j.jmr.2019.03.011
1090-7807/

Hamiltonian theory. Example spectra are presented and advantages and limitations of the approach are discussed in detail.

2. Theory

2.1. X-selective homonuclear decoupling

The BIRD filter was originally designed for homonuclear decoupling of ^{13}C-bound protons that are selectively inverted by the bilinear rotation filter [8,46]. It is especially useful for heteronuclear correlations as implemented in HMQC or HSQC type experiments at natural isotope abundance level, where isotope-filtering is inherent and no additional loss in sensitivity is experienced in BIRD-decoupled acquisition [24,26,27,33,44]. The selective inversion in this case is based on isotope statistics, as each proton bound to a natural abundance ^{13}C nucleus will be surrounded by almost exclusively non-^{13}C-bound protons. If the statistics are changed, e.g. by the application to a uniformly ^{13}C-isotope-labeled molecule, the BIRD-based inversion of protons is not sufficiently selective for neighboring carbons and corresponding homonuclear decoupling is not effective.

For neighboring ^{13}C-nuclei with separated chemical shifts, the application of an X-band-selective BIRD-filter is a potential escape for selective inversion. The corresponding homodecoupling acquisition scheme with an X-band-selective BIRD^{d} filter [46] is shown in Fig. 1: as previously published for natural abundance BIRD-based real-time homonuclear decoupled HSQC sequences [33,36], the conventional heteronuclear decoupling during acquisition is interrupted by BIRD^{d} elements and compensated gradients for the removal of artefacts. As a result, the acquired FID is split into so-called chunks during which homonuclear coupling evolution can be neglected for sufficiently narrow multiplets. Compared to the interferogram type recording of one chunk per scan, which leads to significantly prolonged measurement times, the real-time acquisition of all chunks of an FID per scan [33] is more advantageous for sensitivity (in some cases at the cost of slightly reduced resolution). Almost no additional measurement time is needed, as shown in Fig. 1. The X-selective BIRD decoupling is similar to previously reported BIRD-based pure shift methods [26,33,36,44], with the exception of the X-band-selectivity of the BIRD element that will be discussed below. The chunking time t_c is optimized to a typical value of approximately 12 ms, which is a good compromise for ^{1}H,^{1}H-multiplet widths up to 30 Hz regarding linebroadening due to residual coupling evolution and a minimum amount of selective inversion elements per FID. Please note the definition of t_c in Fig. 1 follows reference [36] as half the total chunk size in the central part of the FID. The real-time acquisition scheme is best used within heteronuclear correlation experiments or in combination with another X-filter-type element. Consequently, the 1D sequence shown in Fig. 1 has been used for the proof of principle data in this article. It consists of an initial X-selective BIRD^{d} element for X-band-selective excitation of selected protons before chunked real-time acquisition with the same X-selective BIRD^{d} filter as the refocusing inversion element. As discussed in the following sections, a REBURP [47] selective refocusing pulse and a BIP [48] or BIBOP [49,50] broadband inversion pulse on the heteronucleus are essential for the best possible performance. The heteronuclear decoupling sequence only needs to cover the selected frequency band, usually significantly reducing the overall rf-energy irradiated, so that acquisition times exceeding 200 ms are easily possible.

2.2. The X-selective BIRD element

In the following, we have a closer look at the effects of the selective pulses considering the example of neighboring carbons in a uniformly ^{13}C-labeled sample as illustrated in Fig. 2: The effective pulse sequence during acquisition can be divided into four different groups of spins. The X-nuclei (^{13}C-nuclei) are separated into

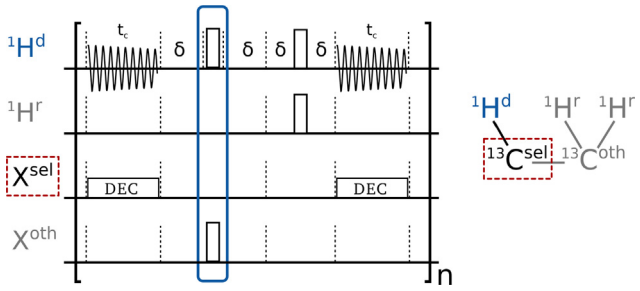

Fig. 2. Schematic illustration of the effective pulse sequence on the different classes of nuclei involved in X-selective BIRD^{d}-based homonuclear decoupling (Fig. 1). H^{d} represents protons that are directly bound to the selected heteronucleus X^{sel} (marked with a dashed, red box), while H^{r} and X^{oth} represent all other protons and heteronuclei, respectively. The blue-boxed pulses represent the idealized effective pulse sequence of the X-selective BIRD^{d} element. While $^{1}J_{XH}$ couplings are suppressed by heteronuclear decoupling, $^{n}J_{XH}$ and $^{n}J_{HH}$ couplings (with n > 1) may evolve during acquisition chunks, but will be refocussed in between chunks, and hence, these couplings are suppressed as long as the sum over all long-range couplings is significantly smaller than $1/t_c$. (For interpretation of the references to colour in this figure legend, the reader is referred to the web version of this article.)

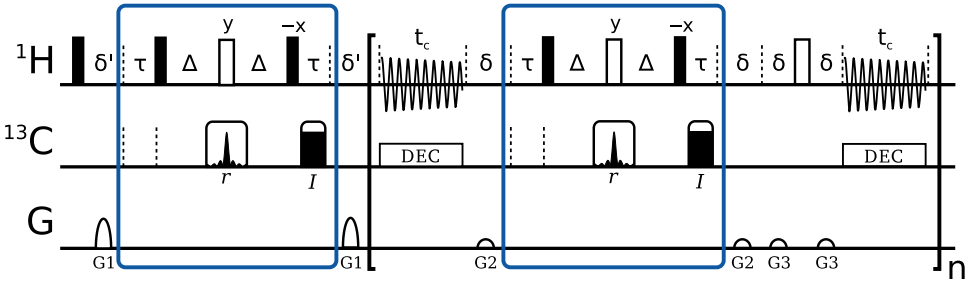

Fig. 1. Pulse sequence used for demonstrating X-(^{13}C)-selective homonuclear decoupling. The initial selection element is followed by chunked real-time acquisition. X-selectivity is achieved by BIRD^{d}-filters using band-selective refocusing on the X-nuclei (BASEREX) (highlighted by blue boxes). All pulses have phase x unless annotated otherwise. A selective REBURP [47] refocusing pulse (r) and a broadband BIP [48] or BIBOP [49,50] inversion pulse (I) with pulse length τ are used for the X-selective BIRD^{d} filter elements as indicated by their rf-amplitude shape. Before acquisition all unwanted signals are destroyed by two spoil-gradients G1 = 60% around the initial BIRD element. Gradients G2 and G3 were set to 7% and 5%, and delays δ' and δ were set to 1.2 ms and 0.5 ms, respectively. Note, that the X-band-selectivity is transferred by the BIRD-filter to the selected X-bound proton and hence, homonuclear proton couplings are suppressed. In order to increase acquisition time, the rf-amplitude for the heteronuclear decoupling sequence (WALTZ16 [51]) was reduced by a factor of 4 compared to the maximum rf-amplitude for broadband heteronuclear decoupling. (For interpretation of the references to colour in this figure legend, the reader is referred to the web version of this article.)

the ones within the X-selected bandwidth, X^{sel}, and all other X nuclei, X^{oth}; equally, for the effect of the BIRD filter elements, protons are divided into directly X^{sel}-bound protons, H^d, and remote protons, H^r, following the established nomenclature introduced in reference [46]. As a result, the X-selected $BIRD^d$ element acts as a 180° pulse on H^d and X^{oth}, while they do nothing on H^r and X^{sel} nuclei. Assuming that the applied rf-amplitude is adapted to only cover the selected X-bandwidth for composite pulse heteronuclear decoupling, X^{oth} also do not experience direct decoupling during chunk acquisition times.

As a result, H^d experiences two 180° pulses per selective inversion element, leading to the desired chemical shift refocusing between chunks. H^r protons instead experience a single 180° pulse between chunks and are consequently decoupled from H^d as long as coupling evolution during chunks can be neglected. In addition, the applied gradients effectively dephase H^r signals. On the heteronuclei, X^{sel} nuclei experience composite pulse decoupling during chunks and effective decoupling in between, as the two pulses of the $BIRD^d$ element cancel each other and the proton 180° pulses provide the requisites for broadband decoupling. X^{oth} nuclei, on the other hand, only experience a single 180° pulse between chunks and therefore are decoupled from H^d protons in an equivalent way to H^r protons under the assumption that coupling constants between H^d and X^{oth} are small and do not show significant evolution during chunk periods.

In the case of using a $BIRD^{d,X}$ element, as has been proposed originally for BIRD-based homodecoupling [26,44], the effective 180° pulse of the BIRD element does not act on X^{oth}, but instead on X^{sel}. Therefore the large $^1J_{CH}$ coupling evolves during 2δ, eventually leading to artefacts for the detected H^d protons. Simultaneously, no pulse is effectively applied on X^{oth}, and since H^d protons experience two 180° pulses in between chunks, there is full coupling evolution during the entire acquisition, if X^{oth} is not within the bandwidth of the applied composite pulse heteronuclear decoupling sequence.

To further evaluate different versions of the BIRD-filter based homonuclear decoupling, we performed simulations using a home-made program based on spin density operator formalism. The acquisition schemes with ideal pulses and gradients for a number of spin system consisting of 4–6 NMR-active spins that represent the most important cases of expected signal forms were simulated. We assumed weakly coupled spins with typical coupling constants of $^2J_{HH} = -11$ Hz, $^3J_{HH} = 5$ Hz and 8 Hz, $^1J_{CH} = 145$, and $^2J_{CH} = -3$ Hz for the different cases. Delays of the BIRD-filter were set to $1/^1J_{CH} = 6.9$ ms for ideal results. We then optimized corresponding chunk times to $t_c = 18.1$ ms and used this timing for all simulations. As we used ideal pulses of zero duration, pulse imperfections were not taken into account. In practice, the application of real pulses with limited rf-amplitudes and the replacement of the central hard 180° pulse in the BIRD element by a selective refocusing pulse [52] has several implications. In particular, the choice of the selective shaped pulse turns out to be crucial, as will be shown in the following section.

The most important results of the simulations are summarized in Fig. 3. Two variants of the broadband BIRD filter: the $BIRD^{d,X}$ and the $BIRD^d$ filter were applied to spin systems representing natural abundance ^{13}CH and $^{13}CH_2$ groups, and to a uniformly ^{13}C-isotope-labeled ^{13}CH-$^{13}CH_2$ group (Fig. 3a). Indeed, homonuclear decoupling is nicely achieved for the natural abundance cases; only the $^2J_{HH}$-coupling within the CH_2 group remains - as both protons are bound to the same carbon. For the uniformly ^{13}C-labeled spin system a fully coupled ^1H-spectrum is obtained, as expected. In addition, a significant difference between the two BIRD-filter types can be seen: while the $BIRD^{d,X}$ filter leads to strong undesired sidebands, the $BIRD^d$ filter shows spectra with strongly reduced artefacts and increased signal intensities.

Further, equivalent simulations using the corresponding X-selective BIRD filters were applied for the uniformly ^{13}C-isotope-labeled ^{13}CH-$^{13}CH_2$ spin system (Fig. 3b). The resulting spectra are very similar to those obtained from the hard pulse BIRD filtered natural abundance simulations. Again, the X-selective $BIRD^d$ filter results in significantly improved spectral quality as compared to the X-selective $BIRD^{d,X}$ filter. For the $BIRD^{d,X}$ case proton signals are further split by $^2J_{CH}$ couplings, as it was assumed that the heteronuclear decoupling multiple pulse sequence did not cover the frequency of the second (neighboring) carbon. In the case of two strongly coupled protons in a selected $^{13}CH_2$ spin system (low right-hand side of Fig. 3b) the typical multiplet with roof-effect is obtained, but still with enhanced signal intensities.

2.3. Selective pulses and J-coupling evolution

A real implementation of the X-selective BIRD homonuclear decoupling scheme involves the application of lengthy band-selective refocusing pulses. As these pulses are usually computer-optimized using a single, uncoupled spin 1/2, coupling evolution in homo- und heteronuclear spin systems are not well-defined *a priori*. In an outstanding examination of selected selective pulses, Lescop, Kern, and Brutscher showed that in INEPT-type transfer elements Q3 and REBURP pulses behave very differently with respect to coupling evolution [52]: while Q3 effectively does not show any evolution of heteronuclear couplings, for REBURP pulses the duration of the pulse shape can be considered being part of the transfer delay. As we were interested in quantifying the coupling evolution contribution during corresponding pulse shapes, we performed calculations of the average Hamiltonian for the selective ^{13}C pulse shapes with and without application of a central hard 180° pulse on protons. The results are shown in Fig. 4: without application of the proton 180° pulse, both pulse shapes provide full refocusing of both chemical shifts and heteronuclear J-coupling evolution (only the case of the REBURP pulse is shown). As can be seen in the top row of Fig. 4, coupling evolution with positive and negative sign comprise the first and the second half of the pulse shape, respectively, and the overall coupling evolution is canceled. This is represented by the vanishing scaling factor $\overline{k(t)}$ of the coupling Hamiltonian within the band-selective region, which is calculated for each offset as the time-average over the entire duration of the pulse shape. If the 180° proton pulse is applied, effective coupling evolution differs significantly. Especially for the REBURP pulse, the sign of the bilinear Hamiltonian in the toggling frame during the second half of the pulse shape is inverted and the overall J-evolution is effectively active for 95% of the duration of the REBURP pulse. The Q3 pulse, instead, shows much lower effective J-evolution, which on-resonance corresponds only to 11% of the pulse duration. By introducing the offset effect as an effective z-rotation into the toggling frame, we also calculated the offset dependence of the effective J-evolution percentage for the two pulse shapes. As can be seen in the rightmost graphs of Fig. 4, the REBURP pulse shape results in a relatively uniform effective J-evolution of 95% over the effective bandwidth of the selective pulse, while we find an effective J-evolution of 11–37% for different offsets for the Q3 pulse.

As different selective bandwidths require selective pulse shapes of different pulse lengths t_p, the following recommendations can be derived for the X-selective BIRD element: for pulses that are shorter than $1/(0.95\ ^1J_{CH})$ we recommend the usage of REBURP pulses for the element, where the actual delays before and after the application of the selective pulse on carbon are reduced by the effective coupling evolution to $1/(2\ ^1J_{CH}) - 0.95\ t_p$. For more selective pulses with longer pulse shapes, in principle the Q3 pulse shape or another pulse shape with very low effective coupling

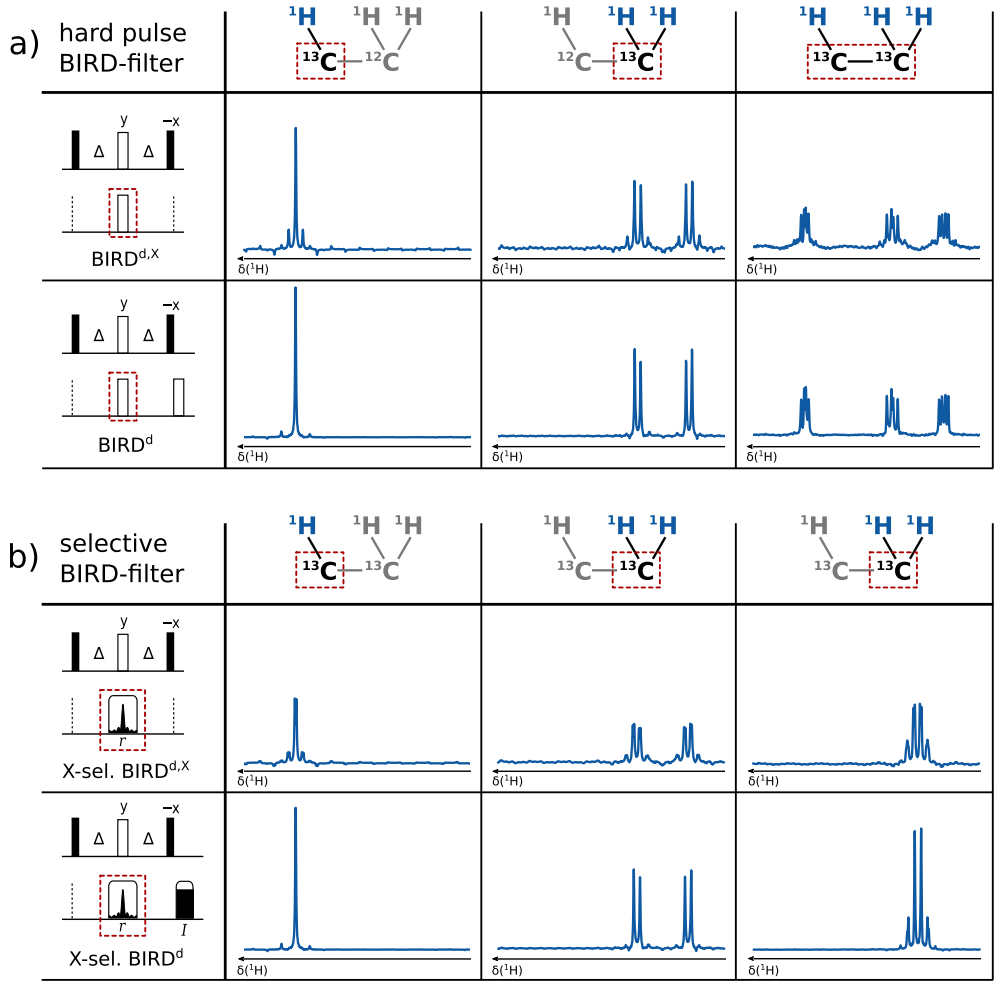

Fig. 3. The acquisition scheme for real-time homonuclear decoupling (Fig. 1) was simulated using broadband and X-selective BIRD^{d}- and BIRD^{d,X}-filters as selective inversion elements. The corresponding selected ^{13}C-nuclei are indicated by red dashed boxes. (a) Only hard pulses are used and natural abundance homonuclear decoupling is best achieved with a BIRD^{d}-filter, while decoupling fails for uniformly ^{13}C-labeled samples. Note the artefacts of BIRD^{d,X} based homodecoupling caused by $^{1}J_{CH}$ coupling evolution during 2·δ. (b) Only uniformly ^{13}C-labeled samples are simulated using a band-selective refocusing pulse (represented by a REBURP shape in red dashed boxes) and a broadband inversion pulse (represented by a constant shape amplitude characteristic for BIBOP/BIP pulses). Only the BIRD^{d}-filter achieves full suppression of all undesired couplings, while the BIRD^{d,X} filter does not suppress $^{n}J_{CH}$ couplings. In the right-hand picture of (b) a spin system with a strongly coupled CH_2-group and corresponding second order artefacts is simulated. In all cases, the delays for the gradients (δ) were assumed twice the experimental value (0.5 ms) to further emphasize the effect of the BIP pulse. The chunk length (t_c) was set to 18.1 ms and couplings were set to the following values: $^{1}J_{CH}$ = 145 Hz; $^{1}J_{CC}$ = 40 Hz; $^{2}J_{HH}$ = -11 Hz; $^{2}J_{CH}$ = -3 Hz; $^{3}J_{HH}$ = 5 and 8 Hz. (For interpretation of the references to colour in this figure legend, the reader is referred to the web version of this article.)

evolution should be used with the corresponding smaller reduction of the delay. For pulse shape durations significantly exceeding 5 ms, however, the approximation of the average Hamiltonian might be very rough and a more accurate simulation of the specific case is suggested. For all experiments shown in the experimental section, refocusing bandwidths were sufficiently wide to use the REBURP pulses.

3. Experiment

For the experimental verification of X-band-selective BIRD-based homonuclear decoupling, the pulse sequence shown in Fig. 1 has been applied to two uniformly ^{13}C-isotope labeled samples readily available in our laboratory, U-^{13}C-glucose (Cambridge Isotope Laboratories) and a U-^{15}N,^{13}C amino acid mixture (Sigma Aldrich) for in vitro biochemical synthesis of proteins. Both samples were prepared in D_2O and have been used for demonstrating the properties of the proposed homonuclear decoupling method.

Spectra of the glucose sample were recorded on a 400 MHz Bruker Avance III HD spectrometer equipped with a dual channel broadband, inverse-detected (BBI) probehead. 2048 complex data points with a spectral width of 6 kHz (resulting FID resolution of 2.93 Hz) were acquired. For the homodecoupled spectra the chunk number was set to n = 14 (see Fig. 1 for pulse sequence details). Spectra recorded on the amino acid mixture were recorded on a 600 MHz Bruker Avance III spectrometer equipped with a cryogenically cooled ^{1}H,^{13}C,^{15}N triple resonance (TCI) probehead. For all 1Ds a spectral width of 7.2 kHz was chosen and the carrier frequency set to 4.7 ppm. While the regular 1D was recorded with 8192 complex points (FID resolution of 0.88 Hz), the homodecoupled 1Ds involved 2048 complex points (FID resolution of 3.51 Hz) with a chunk number of n = 12.

3.1. Proof of principle

For the uniformly ^{13}C-labeled glucose initial optimization of the BIRD elements and other settings regarding the homonuclear decoupling scheme have been performed. The anomeric centers of α- and β-glucose are particularly separated from other parts of the molecule regarding both ^{1}H and ^{13}C chemical shifts, which

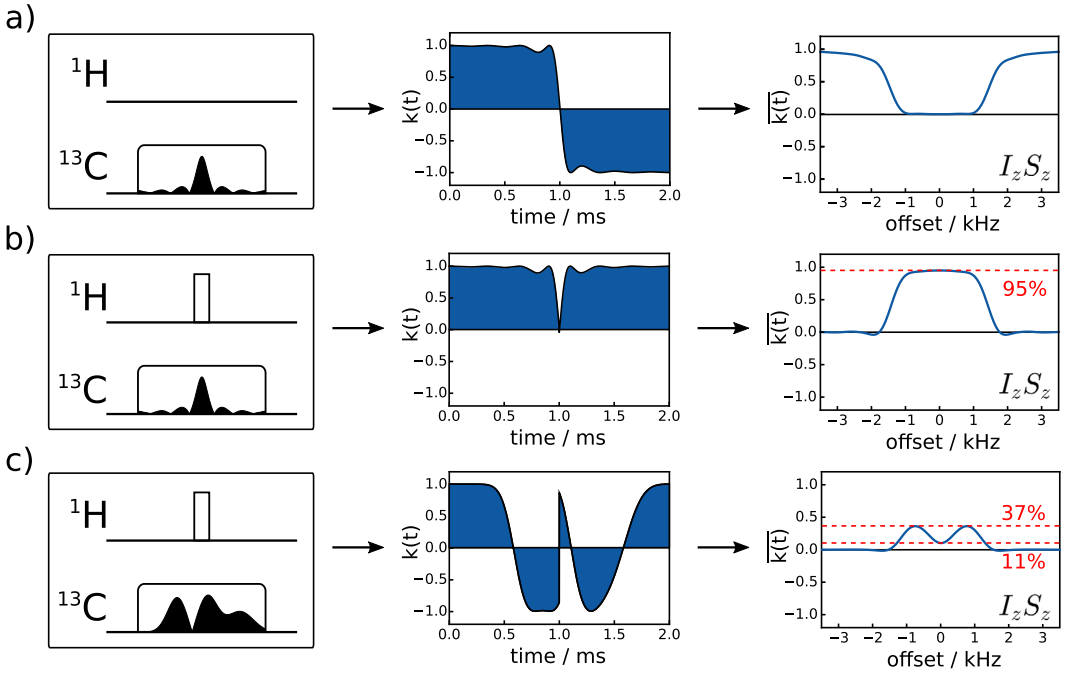

Fig. 4. REBURP (a,b) and Q3 (c) shaped pulses (pulse shape amplitudes and effective simulated sequence, left column) for selective refocussing were simulated on-resonance in the toggling frame (middle column) and the respective time-averaged Hamiltonian for the heteronuclear coupling is plotted against the offset (right column). First, REBURP was simulated (a) without and (b) with an ideal π-pulse on ^{1}H. In (c) the Q3 is simulated with an ideal π-pulse applied on ^{1}H; in comparison to (b) one can see that the effective coupling evolution is not only smaller in size but also less uniform.

guaranteed a straightforward experimental setup. The selection of other C-H moieties would be possible, but second order artefacts due to insufficient chemical shift separation would lead to non-ideal evolution during the BIRD-elements and inevitably result in distorted signals. A selective REBURP pulse of 5 ms duration has been used for a carbon selected region of 800 Hz centered at 94 ppm. To monitor the sensitivity of homodecoupling to the transfer delay within the BIRD elements, ideal delays for one-bond couplings of 125 Hz, 145 Hz, 160 Hz, 170 Hz, 180 Hz, and 200 Hz were implemented, taking into account the considerations on the REBURP selective refocusing pulse of the previous section. The J-misset behaviour of a BIRD-element in real-time homonuclear decoupling has previously been reported in [53]. The results in Fig. 5 represent the expected curve, which is a clear demonstration for the importance to include the coherence transfer during the shaped REBURP pulse into the overall BIRD-delay calculation. Compared to the conventional 1D spectrum (Fig. 5a), homodecoupled spectra for the various delays using a BIRD^d element are shown in Fig. 5b. Clearly the ^{1}H,^{1}H-multiplets collapse in all homodecoupled spectra, but the linewidths and signal intensities vary significantly between spectra recorded with different delays. Best results are obtained for delays that match the optimal conditions for the actual one-bond coupling constants of $^1J_{CH}(\alpha)$ = 170 Hz and $^1J_{CH}(\beta)$ = 161 Hz, applying the correction for the 5 ms selective REBURP pulse as derived in the previous section. However, decoupling performance is still well tolerable for deviations of couplings in the range of ±20% of the nominal coupling used for calculating the delay.

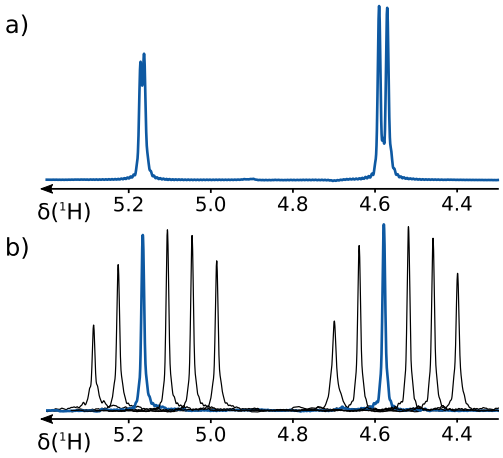

Fig. 5. The effect of X-selective homonuclear and heteronuclear decoupled 1D spectra of the anomeric centers of uniformly ^{13}C-labelled α- and β-Glucose. (a) Standard acquisition with heteronuclear decoupling. (b) Real-time homonuclear decoupling using a BIRD^d-filter as the selective inversion element with a chunk length of t_c = 12.2 ms. BIRD delays were calculated from Δ = 1/(2•J) where J was varied (from left to right: 125 Hz, 145 Hz, 160 Hz, 170 Hz, 180 Hz, 200 Hz) and the duration of the selective pulse was considered according to text. While the spectrum for *J* = 160 Hz, the optimum value for the anomeric center of β-glucose, is shown in bold blue with correct chemical shifts, all other homodecoupled spectra have been shifted for better visibility. All spectra have been recorded and processed under identical conditions using a 5 ms selective REBURP pulse for bandselective inversion of the carbon spins with compensated delays, so that resulting signal intensities can be directly compared. Measured $^1J_{CH}$ couplings were determined experimentally to be 161 Hz for β-glucose (4.58 ppm) and 170 Hz for α-glucose (5.17 ppm).

3.2. X-band selectivity

Another important aspect are the X-band selectivity properties of the proposed approach. For this purpose we examined a more complex sample existing in our laboratory, a uniformly ^{15}N,^{13}C-labeled amino acid mixture. The 1D spectrum of the Hα region clearly shows its crowdedness with extensive overlap (Fig. 6a). Band-selectivity on the proton channel would most likely allow homonuclear decoupling of most of the signals, but carbon selectivity can be achieved more easily. In addition, as mentioned before, heteronuclear long-range coupling evolution is easily suppressed with the X-selective BIRD^d element using broadband

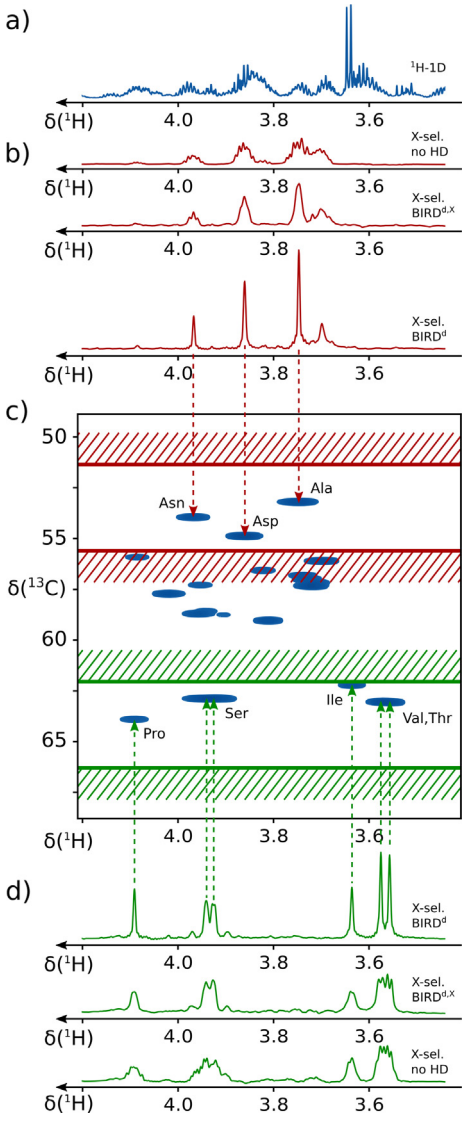

Fig. 6. The ^{1}H-1D spectrum (a) and the constant time HSQC (c) of the Hα,Cα-region of a uniformly ^{13}C,^{15}N-labeled amino acid mixture is shown together with multiple X-band-selective ^{1}H-1Ds (b,d), where different acquisition schemes are tested. Selected amino acid types are highlighted. While in (a) a ^{1}H-1D with standard acquisition (no homonuclear decoupling, 8192 complex points per FID resulting in 0.88 Hz resolution) is shown, in (b) and (d) the red and the green area, respectively, is selected by corresponding selective refocusing pulses of the BIRD elements. Spectra without homonuclear decoupling (no HD) as well as spectra with homonuclear decoupling using X-selective BIRD^{d,X} or BIRD^d elements (see Fig. 3 for a theoretical comparison) are shown. The 1Ds were recorded with 2048 complex points, resulting in a digital resolution of 3.51 Hz. The chunk length (t_c) was set to 11.8 ms and the length of the selective REBURP pulse to 6 ms. Line broadening of 0.9 Hz and linear prediction as mentioned in [54] was applied to all 1Ds in Topspin before the spectra were plotted using nmrglue [55].

inversion pulses, while HOBS or BASHD sequences allow this suppression only if high power broadband heteronuclear decoupling sequences are applied that cover the entire range of X-nuclear chemical shifts. We chose two arbitrary, relatively separated carbon chemical shift regions, which we excited selectively followed by acquisition with no homodecoupling, X-selective homodecoupling using BIRD^{d,X} elements, and X-selective homodecoupling using BIRD^d elements (Fig. 6b,d). The X-selective excitation as well as the decoupling scheme selects spins within the bandwidth of the selective REBURP pulses. Artefacts and reduced signal intensities occur only for few signals in the transition region of the selective pulses applied (indicated by ruled areas in Fig. 6c). Clearly, the X-selective excitation simplifies spectra considerably, but multiplets are very broad with low overall sensitivity. X-selective BIRD^{d,X} homodecoupling leads to simplified multiplets and a small enhancement in sensitivity, but non-refocused heteronuclear long-range couplings still lead to severely broadened lines. X-band-selective BIRD^d homodecoupling finally leads to narrow lines with strongly enhanced signal intensities. The worst situation for X-band-selective BIRD decoupling can be seen with the CH_2 group of serine in Fig. 6d, where the geminal ^{1}H,^{1}H-coupling is not decoupled by the BIRD element and the spin system in addition is influenced by second order artefacts of the effective ABX spin system (For a qualitative simulation of the spin system see Fig. 3b). The most convincing example in Fig. 6d, on the other hand, is maybe the separation of the Hα protons of valine and threonine: while the signals show severe overlap even in the two-dimensional spectrum, X-selective BIRD^d homodecoupling allows a clear distinction of the two signals.

4. Discussion

Selective inversion elements are at the heart of modern homonuclear decoupling approaches based on chunked FIDs. For broadband decoupling the original Zangger-Sterk element [22] as well as the PSYCHE element [41] and the BIRD filter [8,26,46] are being used, while ^{1}H-selective pulses have been used in band-selective BASHD [43] and HOBS [42] approaches. The novel selective inversion element for homonuclear decoupling introduced in this article combines a BIRD^d element with the application of band-selective refocusing on the X-nucleus. As such, the X-selective BIRD decoupling scheme allows the selection of decoupled spins *via* a selected bandwidth of the heteronucleus X. Especially in cases of coupled protons bound to the same type of heteronucleus, as is, for example, typically the case in uniformly ^{13}C-isotope labeled compounds, the introduced homonuclear decoupling scheme is applicable where conventional BIRD decoupling does not apply. As such, the tool box of homodecoupling techniques is generally extended and applications in areas with routine isotope labeling of samples can be foreseen.

Compared to other band-selective methods like HOBS and BASHD, the X-selective BIRD homodecoupling has the disadvantage that only spins bound to the selected X-nuclei can be recorded. On the other hand, it allows the usage of heteronuclear dispersion for enhanced selectivity, opening new possibilities for tailoring desired decoupling properties. As X-selective BIRD homodecoupling can be applied in real-time acquisition, no loss of signal intensity is experienced in isotope-labeled samples and even slight gains might be expected when losses during the BIRD-elements can be minimized.

Looking at details of the BIRD-based homodecoupling, both BIRD^{d,X} and BIRD^d elements can be used. Initially, the BIRD^{d,X} filter has been introduced to obtain pure shift spectra [26,44], before the Frydman group introduced a BIRD^d filter with two adiabatic inversion pulses [33], and we had a detailed look into the properties of the two approaches. As has been shown previously in [53] and also here in the theory section, the BIRD^d element has significant advantages over the BIRD^{d,X} element, as it allows full decoupling of the large one-bond couplings between chunks. In isotope labeled samples, the BIRD^d element also effectively decouples the many heteronuclear long-range couplings between chunks, while the effective 180° pulse on the X pulse in the BIRD^{d,X} case leads to coupling evolution during gradient periods around the BIRD and at offsets where the heteronuclear composite pulse decoupling during chunks is not sufficiently active. Especially in real-time experiments this difference is strongly noticeable and a clear preference for the BIRD^d-based approach is given.

Concerning the applicability of the X-selective BIRD^{d} homodecoupling, it should be noted, that composite pulse heteronuclear decoupling only has to cover the X-selected bandwidth, while all other homodecoupling approaches require broadband heteronuclear decoupling over the whole spectral width of the X-nucleus. This well-received property originates from the simultaneous effective chunked decoupling of ^{1}H,^{1}H- as well as long-range ^{1}H,^{13}C-couplings inherent to the X-selective BIRD^{d} element.

Regarding the actual setup of X-selective BIRD homonuclear decoupling, several details regarding pulses and timing have to be considered. While most pulses only need to cover the selected bandwidth, the second 180° X-pulse in the BIRD^{d} element needs to cover the bandwidth of the entire X-nucleus, i.e. the entire ca. 200 ppm spectral width in the case of ^{13}C. For this purpose we had to introduce an essential BIP [48] or BIBOP [49,50] broadband inversion pulse at the corresponding position to avoid similar artefacts as with the application of a BIRD^{d,X} element.

Also the exact timing of the delays within the X-selective BIRD elements is crucial and depends heavily on the selective refocusing pulse shape used. As has been pointed out previously [52,56], the simultaneous application of pulses on two channels may have profound effects on coupled spins, as it alters coupling evolution properties. As such, it turned out that REBURP selective refocusing pulses have ideal properties for most cases with coupling evolution taking place during 95% of the actual length of the pulse shape. Accordingly, the delays in the experiment have to be adjusted (shortened) to minimize signal loss during the many BIRD elements applied during acquisition.

5. Conclusion

An X-band-selective BIRD^{d} filter has been introduced as a selective inversion element for homonuclear decoupling. The effect of the BIRD element has been studied in detail and all aspects regarding required bandwidths and timings with respect to selective shape pulse length have been discussed. Finally, initial examples for the potential usefulness of the approach regarding ^{13}C isotope labeled samples have been demonstrated experimentally. Applications to small proteins, for example, theoretically may lead to significantly enhanced signal widths in Hα protons, as these protons for most amino acid types are split by three $^{3}J_{H}\alpha_{H}$, two $^{3}J_{H}\alpha_{C}$ and several more two-bond couplings, resulting generally in unresolved multiplet contributions larger 20 Hz. The situation is similar for H1′ and aromatic protons in nucleid acids, for which the proposed BASEREX decoupling scheme will allow increased signal intensities and resolution. Further studies on proteins and small RNA are currently under investigation.

Acknowledgement

The authors thank the Deutsche Forschungsgemeinschaft (projects LU 835/11-1, LU 835/13-1, and instrumentation facility Pro^{2}NMR), as well as the HGF programme Biointerfaces in Technology and Medicine for financial support. Support by the ELTE Institutional Excellence Program (1783-3/2018/FEKUTSRAT) of the Hungarian Ministry of Human Capacities and the National Research, Development and Innovation Office, Hungary (NKFI K124900) is acknowledged.

References

[1] W.A. Anderson, R. Freeman, Influence of a Second Radiofrequency Field on High-Resolution Nuclear Magnetic Resonance Spectra, J. Chem. Phys. 37 (1962) 85–103, https://doi.org/10.1063/1.1732980.
[2] R.R. Ernst, Nuclear magnetic double resonance with an incoherent radio-frequency field, J. Chem. Phys. 45 (1966) 3845–3861, https://doi.org/10.1063/1.1727409.
[3] Ē. Kupče, R. Freeman, G. Wider, K. Wüthrich, Suppression of cycling sidebands using bi-level adiabatic decoupling, J. Magn. Reson. 122 (1996) 81–84, https://doi.org/10.1006/jmra.1996.0180.
[4] M.H. Levitt, R. Freeman, T. Frenkiel, Broadband decoupling in high-resolution nuclear magnetic resonance spectroscopy, in: Methods Exp. Phys., 1983, pp. 47–110. http://doi.org/10.1016/B978-0-12-025511-5.50008-6.
[5] F. Schilling, L.R. Warner, N.I. Gershenzon, T.E. Skinner, M. Sattler, S.J. Glaser, Next-generation heteronuclear decoupling for high-field biomolecular NMR spectroscopy, Angew. Chem., Int. Ed. 53 (2014) 4475–4479, https://doi.org/10.1002/anie.201400178.
[6] W.P. Aue, J. Karhan, R.R. Ernst, Homonuclear broad band decoupling and two-dimensional J-resolved NMR spectroscopy, J. Chem. Phys. 64 (1976) 4226–4227, https://doi.org/10.1063/1.431994.
[7] A. Bax, R. Freeman, Investigation of complex networks of spin-spin coupling by two-dimensional NMR, J. Magn. Reson. 44 (1981) 542–561, https://doi.org/10.1016/0022-2364(81)90287-0.
[8] J.R. Garbow, D.P. Weitekamp, A. Pines, Bilinear rotation decoupling of homonuclear scalar interactions, Chem. Phys. Lett. 93 (1982) 504–509, https://doi.org/10.1016/0009-2614(82)83229-6.
[9] S. Simova, H. Sengstschmid, R. Freeman, Proton chemical-shift spectra, J. Magn. Reson. 124 (1997) 104–121, https://doi.org/10.1006/jmre.1996.1001.
[10] M.J. Thrippleton, R.A.E. Edden, J. Keeler, Suppression of strong coupling artefacts in J-spectra, J. Magn. Reson. 174 (2005) 97–109, https://doi.org/10.1016/j.jmr.2005.01.012.
[11] B. Luy, Adiabatic z -filtered J -spectroscopy for absorptive homonuclear decoupled spectra, J. Magn. Reson. 201 (2009) 18–24, https://doi.org/10.1016/j.jmr.2009.07.025.
[12] B. Görling, S. Bräse, B. Luy, HR-HSBC: Measuring heteronuclear one-bond couplings with enhanced resolution, Magn. Reson. Chem. 50 (2012) S58–S62, https://doi.org/10.1002/mrc.3878.
[13] P. Sakhaii, B. Haase, W. Bermel, Broadband homodecoupled heteronuclear multiple bond correlation spectroscopy, J. Magn. Reson. 228 (2013) 125–129, https://doi.org/10.1016/j.jmr.2012.12.018.
[14] B. Görling, W. Bermel, S. Bräse, B. Luy, Homonuclear decoupling by projection reconstruction, Magn. Reson. Chem. 56 (2018) 1006–1020, https://doi.org/10.1002/mrc.4784.
[15] D. Carnevale, T.F. Segawa, G. Bodenhausen, Polychromatic decoupling of a manifold of homonuclear scalar interactions in solution-state NMR, Chem. - Eur. J. 18 (2012) 11573–11576, https://doi.org/10.1002/chem.201200481.
[16] J. Farjon, W. Bermel, C. Griesinger, Resolution enhancement in spectra of natural products dissolved in weakly orienting media with the help of ^{1}H homonuclear dipolar decoupling during acquisition: application to ^{1}H–^{13}C dipolar couplings measurements, J. Magn. Reson. 180 (2006) 72–82, https://doi.org/10.1016/j.jmr.2006.01.006.
[17] A. Hammarström, G. Otting, Improved spectral resolution in ^{1}H NMR spectroscopy by homonuclear semiselective shaped pulse decoupling during acquisition, J. Am. Chem. Soc. 116 (1994) 8847–8848, https://doi.org/10.1021/ja00098a070.
[18] J.P. Jesson, P. Meakin, G. Kneissel, Homonuclear decoupling and peak elimination in Fourier transform nuclear magnetic resonance, J. Am. Chem. Soc. 95 (1973) 618–620, https://doi.org/10.1021/ja00783a068.
[19] Ē. Kupče, R. Freeman, Polychromatic Selective Pulses, J. Magn. Reson. 102 (1993) 122–126, https://doi.org/10.1006/jmra.1993.1079.
[20] C.W. Vander Kooi, Ē. Kupče, E.R.P. Zuiderweg, M. Pellecchia, Line narrowing in spectra of proteins dissolved in a dilute liquid crystalline phase by band-selective adiabatic decoupling: application to $^{1}H^{N}$–^{15}N residual dipolar coupling measurements, J. Biomol. NMR. 15 (1999) 335–338, https://doi.org/10.1023/A: 1008387305293.
[21] J. Weigelt, A. Hammarström, W. Bermel, G. Otting, Removal of zero-quantum coherence in protein NMR spectra using SESAM decoupling and suppression of decoupling sidebands, J. Magn. Reson. 110 (1996) 219–224, https://doi.org/10.1006/jmrb.1996.0036.
[22] K. Zangger, H. Sterk, Homonuclear broadband-decoupled NMR spectra, J. Magn. Reson. 124 (1997) 486–489, https://doi.org/10.1006/jmre.1996.1063.
[23] G.A. Morris, J.A. Aguilar, R. Evans, S. Haiber, M. Nilsson, True chemical shift correlation maps: A TOCSY experiment with pure shifts in both dimensions, J. Am. Chem. Soc. 132 (2010) 12770–12772, https://doi.org/10.1021/ja1039715.
[24] T. Reinsperger, B. Luy, Homonuclear BIRD-decoupled spectra for measuring one-bond couplings with highest resolution: CLIP/CLAP-RESET and constant-time-CLIP/CLAP-RESET, J. Magn. Reson. 239 (2014) 110–120, https://doi.org/10.1016/j.jmr.2013.11.015.
[25] M. Nilsson, G.A. Morris, Pure shift proton DOSY: diffusion-ordered ^{1}H spectra without multiplet structure, Chem. Commun. (2007) 933, https://doi.org/10.1039/b617761a.
[26] P. Sakhaii, B. Haase, W. Bermel, Experimental access to HSQC spectra decoupled in all frequency dimensions, J. Magn. Reson. 199 (2009) 192–198, https://doi.org/10.1016/j.jmr.2009.04.016.
[27] I. Timári, L. Kaltschnee, A. Kolmer, R.W. Adams, M. Nilsson, C.M. Thiele, G.A. Morris, K.E. Kövér, Accurate determination of one-bond heteronuclear coupling constants with "pure shift" broadband proton-decoupled CLIP/CLAP-HSQC experiments, J. Magn. Reson. 239 (2014) 130–138, https://doi.org/10.1016/j.jmr.2013.10.023.
[28] S. Glanzer, K. Zangger, Directly decoupled diffusion-ordered NMR spectroscopy for the analysis of compound mixtures, Chem. - Eur. J. 20 (2014) 11171–11175, https://doi.org/10.1002/chem.201402920.

[29] N. Lokesh, S.R. Chaudhari, N. Suryaprakash, Quick re-introduction of selective scalar interactions in a pure-shift NMR spectrum, Chem. Commun. 50 (2014) 15597–15600, https://doi.org/10.1039/C4CC06772J.
[30] M. Reller, S. Wesp, M.R.M. Koos, M. Reggelin, B. Luy, Biphasic liquid crystal and the simultaneous measurement of isotropic and anisotropic parameters by spatially resolved NMR spectroscopy, Chem. - Eur. J. 23 (2017) 13351–13359, https://doi.org/10.1002/chem.201702126.
[31] B. Sathyamoorthy, D.M. Parish, G.T. Montelione, R. Xiao, T. Szyperski, Spatially selective heteronuclear multiple-quantum coherence spectroscopy for biomolecular NMR Studies, ChemPhysChem. 15 (2014) 1872–1879, https://doi.org/10.1002/cphc.201301232.
[32] L. Kaltschnee, A. Kolmer, I. Timári, V. Schmidts, R.W. Adams, M. Nilsson, K.E. Kövér, G.A. Morris, C.M. Thiele, "Perfecting" pure shift HSQC: full homodecoupling for accurate and precise determination of heteronuclear couplings, Chem. Commun. 50 (2014) 15702–15705, https://doi.org/10.1039/C4CC04217D.
[33] A. Lupulescu, G.L. Olsen, L. Frydman, Toward single-shot pure-shift solution ^{1}H NMR by trains of BIRD-based homonuclear decoupling, J. Magn. Reson. 218 (2012) 141–146, https://doi.org/10.1016/j.jmr.2012.02.018.
[34] N.H. Meyer, K. Zangger, Simplifying proton NMR spectra by instant homonuclear broadband decoupling, Angew. Chem., Int. Ed. 52 (2013) 7143–7146, https://doi.org/10.1002/anie.201300129.
[35] N. Helge Meyer, K. Zangger, Enhancing the resolution of multi-dimensional heteronuclear NMR spectra of intrinsically disordered proteins by homonuclear broadband decoupling, Chem. Commun. 50 (2014) 1488–1490, https://doi.org/10.1039/C3CC48135B.
[36] L. Paudel, R.W. Adams, P. Király, J.A. Aguilar, M. Foroozandeh, M.J. Cliff, M. Nilsson, P. Sándor, J.P. Waltho, G.A. Morris, Simultaneously enhancing spectral resolution and sensitivity in heteronuclear correlation NMR spectroscopy, Angew. Chem., Int. Ed. 52 (2013) 11616–11619, https://doi.org/10.1002/anie.201305709.
[37] I. Timári, L. Kaltschnee, M.H. Raics, F. Roth, N.G.A. Bell, R.W. Adams, M. Nilsson, D. Uhrín, G.A. Morris, C.M. Thiele, K.E. Kövér, Real-time broadband proton-homodecoupled CLIP/CLAP-HSQC for automated measurement of heteronuclear one-bond coupling constants, RSC Adv. 6 (2016) 87848–87855, https://doi.org/10.1039/C6RA14329F.
[38] L. Castañar, T. Parella, Broadband 1 H homodecoupled NMR experiments: recent developments, methods and applications, Magn. Reson. Chem. 53 (2015) 399–426, https://doi.org/10.1002/mrc.4238.
[39] K. Zangger, Pure shift NMR, Prog. Nucl. Magn. Reson. Spectrosc. 86–87 (2015) 1–20, https://doi.org/10.1016/j.pnmrs.2015.02.002.
[40] D. Sinnaeve, M. Foroozandeh, M. Nilsson, G.A. Morris, A General method for extracting individual coupling constants from crowded 1 H NMR spectra, Angew. Chem., Int. Ed. 55 (2016) 1090–1093, https://doi.org/10.1002/anie.201508691.
[41] M. Foroozandeh, R.W. Adams, N.J. Meharry, D. Jeannerat, M. Nilsson, G.A. Morris, Ultrahigh-resolution NMR spectroscopy, Angew. Chem., Int. Ed. 53 (2014) 6990–6992, https://doi.org/10.1002/anie.201404111.
[42] L. Castañar, P. Nolis, A. Virgili, T. Parella, Full sensitivity and enhanced resolution in homodecoupled band-selective NMR experiments, Chem. - Eur. J. 19 (2013) 17283–17286, https://doi.org/10.1002/chem.201303235.
[43] J. Ying, J. Roche, A. Bax, Homonuclear decoupling for enhancing resolution and sensitivity in NOE and RDC measurements of peptides and proteins, J. Magn. Reson. 241 (2014) 97–102, https://doi.org/10.1016/j.jmr.2013.11.006.
[44] J.A. Aguilar, M. Nilsson, G.A. Morris, Simple proton spectra from complex spin systems: pure shift NMR spectroscopy using BIRD, Angew. Chem., Int. Ed. 50 (2011) 9716–9717, https://doi.org/10.1002/anie.201103789.
[45] J. Furrer, M. John, H. Kessler, B. Luy, J-Spectroscopy in the presence of residual dipolar couplings: determination of one-bond coupling constants and scalable resolution, J. Biomol. NMR 37 (2007) 231–243, https://doi.org/10.1007/s10858-006-9130-x.
[46] D. Uhrín, T. Liptaj, K.E. Kövér, Modified BIRD pulses and design of heteronuclear pulse sequences, J. Magn. Reson. 101 (1993) 41–46, https://doi.org/10.1006/jmra.1993.1005.
[47] H. Geen, R. Freeman, Band-selective radiofrequency pulses, J. Magn. Reson. 93 (1991) 93–141, https://doi.org/10.1016/0022-2364(91)90034-Q.
[48] M.A. Smith, H. Hu, A.J. Shaka, Improved broadband inversion performance for NMR in liquids, J. Magn. Reson. 151 (2001) 269–283, https://doi.org/10.1006/jmre.2001.2364.
[49] K. Kobzar, T.E. Skinner, N. Khaneja, S.J. Glaser, B. Luy, Exploring the limits of broadband excitation and inversion pulses, J. Magn. Reson. 170 (2004) 236–243, https://doi.org/10.1016/j.jmr.2004.06.017.
[50] K. Kobzar, T.E. Skinner, N. Khaneja, S.J. Glaser, B. Luy, Exploring the limits of broadband excitation and inversion: II. Rf-power optimized pulses, J. Magn. Reson. 194 (2008) 58–66, https://doi.org/10.1016/j.jmr.2008.05.023.
[51] A.J. Shaka, J. Keeler, T. Frenkiel, R. Freeman, An improved sequence for broadband decoupling: WALTZ-16, J. Magn. Reson. 52 (1983) 335–338, https://doi.org/10.1016/0022-2364(83)90207-X.
[52] E. Lescop, T. Kern, B. Brutscher, Guidelines for the use of band-selective radiofrequency pulses in hetero-nuclear NMR: Example of longitudinal-relaxation-enhanced BEST-type ^{1}H–^{15}N correlation experiments, J. Magn. Reson. 203 (2010) 190–198, https://doi.org/10.1016/j.jmr.2009.12.001.
[53] P. Király, M. Nilsson, G.A. Morris, Practical aspects of real-time pure shift HSQC experiments, Magn. Reson. Chem. 56 (2018) 993–1005, https://doi.org/10.1002/mrc.4704.
[54] P. Király, G. Morris, L. Quanxiu, M. Nilsson, Sharpening up your spectra: broadband homonuclear decoupling in HSQC by real-time pure shift acquisition, Synlett (2019), https://doi.org/10.1055/s-0037-1612057.
[55] J.J. Helmus, C.P. Jaroniec, Nmrglue: an open source Python package for the analysis of multidimensional NMR data, J. Biomol. NMR 55 (2013) 355–367, https://doi.org/10.1007/s10858-013-9718-x.
[56] S. Ehni, B. Luy, BEBE^{tr} and BUBI: J-compensated concurrent shaped pulses for ^{1}H–^{13}C experiments, J. Magn. Reson. 232 (2013) 7–17, https://doi.org/10.1016/j.jmr.2013.04.007.